

# An Organodiselenide Comediator to Facilitate Sulfur Redox Kinetics in Lithium–Sulfur Batteries

Meng Zhao, Xiang Chen, Xi-Yao Li, Bo-Quan Li, and Jia-Qi Huang\*

**Lithium–sulfur (Li–S) batteries are considered as promising next-generation energy storage devices due to their ultrahigh theoretical energy density, where soluble lithium polysulfides are crucial in the Li–S electrochemistry as intrinsic redox mediators. However, the poor mediation capability of the intrinsic polysulfide mediators leads to sluggish redox kinetics, further rendering limited rate performances, low discharge capacity, and rapid capacity decay. Here, an organodiselenide, diphenyl diselenide (DPDSe), is proposed to accelerate the sulfur redox kinetics as a redox comediator. DPDSe spontaneously reacts with lithium polysulfides to generate lithium phenylseleno polysulfides (LiPhSePSs) with improved redox mediation capability. The as-generated LiPhSePSs afford faster sulfur redox kinetics and increase the deposition dimension of lithium sulfide. Consequently, the DPDSe comediator endows Li–S batteries with superb rate performance of 817 mAh g<sup>-1</sup> at 2 C and remarkable cycling stability with limited anode excess. Moreover, Li–S pouch cells with the DPDSe comediator achieve an actual initial energy density of 301 Wh kg<sup>-1</sup> and 30 stable cycles. This work demonstrates a novel redox comediators strategy with an effective organodiselenide comediator to facilitate the sulfur redox kinetics under pouch cell conditions and inspires further exploration in mediating Li–S kinetics for practical high-energy-density batteries.**

friendliness.<sup>[2]</sup> Generally, the sulfur redox reactions undergo from solid elemental sulfur to soluble lithium polysulfides and finally to solid lithium sulfide (Li<sub>2</sub>S) during discharging, where the charging process is in reverse.<sup>[3]</sup> However, the solid sulfur and Li<sub>2</sub>S are electronic and ionic insulators, while the dissolved lithium polysulfides tend to shuttle between the cathode and the anode.<sup>[4]</sup> Moreover, the conversions between the solid and dissolved species inevitably result in dramatic phase migration and active material loss.<sup>[5]</sup> Therefore, despite the high theoretical specific capacity of 1672 mAh g<sup>-1</sup> between S<sub>8</sub> and Li<sub>2</sub>S, the actual specific capacity is relatively low and decays rapidly with high rates or along cycling. The poor sulfur redox kinetics constitutes the main challenge to limit the performances of Li–S batteries.

To address the above challenges, a redox mediation strategy is proposed to promote the sulfur redox kinetics.<sup>[6]</sup> Typically, redox mediators function through regulating the chemical reactions of the sulfur species parallel to but coupled with the electrochemical processes.<sup>[7]</sup> For instance, the comproportionation between Li<sub>2</sub>S<sub>6</sub> and Li<sub>2</sub>S to regenerate Li<sub>2</sub>S<sub>4</sub> during discharging regulates the deposition capacity and morphology of solid Li<sub>2</sub>S, which has a significant influence on the reversibility of Li<sub>2</sub>S deposition/dissolution capacity corresponding to the second discharge plateau during cycling.<sup>[8]</sup> Similarly, the lithium polysulfides with moderate oxidation state can all function as intrinsic redox mediators in working Li–S batteries to regulate the sulfur redox kinetics and determine the battery performances.<sup>[9]</sup> Nevertheless, the redox mediation capability of the intrinsic polysulfide mediators is often beyond satisfactory under working conditions.<sup>[10]</sup> Therefore, promoting the redox mediation capability to accelerate the sulfur redox kinetics is highly regarded to realize high-performance Li–S batteries especially under practical conditions with high sulfur loading, low electrolyte volume, and limited lithium excess.

The introduction of extrinsic redox mediators constitutes a facile approach to promote sulfur redox kinetics following the redox mediation mechanism.<sup>[11]</sup> Pentamethylferrocene was first adopted as an extrinsic redox mediator to promote Li<sub>2</sub>S oxidation, during which process a high energy barrier is required to be overcome.<sup>[12]</sup> Anthraquinone derivatives have also been confirmed to effectively mediate the Li<sub>2</sub>S oxidation process.<sup>[13]</sup> On

The rapid growth of global energy demand drives the development of next-generation rechargeable batteries with high energy densities.<sup>[1]</sup> Lithium–sulfur (Li–S) batteries have attracted tremendous attention due to their high theoretical energy density of 2600 Wh kg<sup>-1</sup> and the superiority of sulfur including earth abundance, low cost, and environmental

M. Zhao, Dr. B.-Q. Li, Prof. J.-Q. Huang  
School of Materials Science and Engineering  
Beijing Institute of Technology  
Beijing 100081, China  
E-mail: jqhuang@bit.edu.cn

M. Zhao, Dr. B.-Q. Li, Prof. J.-Q. Huang  
Advanced Research Institute of Multidisciplinary Science  
Beijing Institute of Technology  
Beijing 100081, China

Dr. X. Chen, X.-Y. Li  
Beijing Key Laboratory of Green Chemical Reaction  
Engineering and Technology  
Department of Chemical Engineering  
Tsinghua University  
Beijing 100084, China

 The ORCID identification number(s) for the author(s) of this article can be found under <https://doi.org/10.1002/adma.202007298>.

DOI: 10.1002/adma.202007298

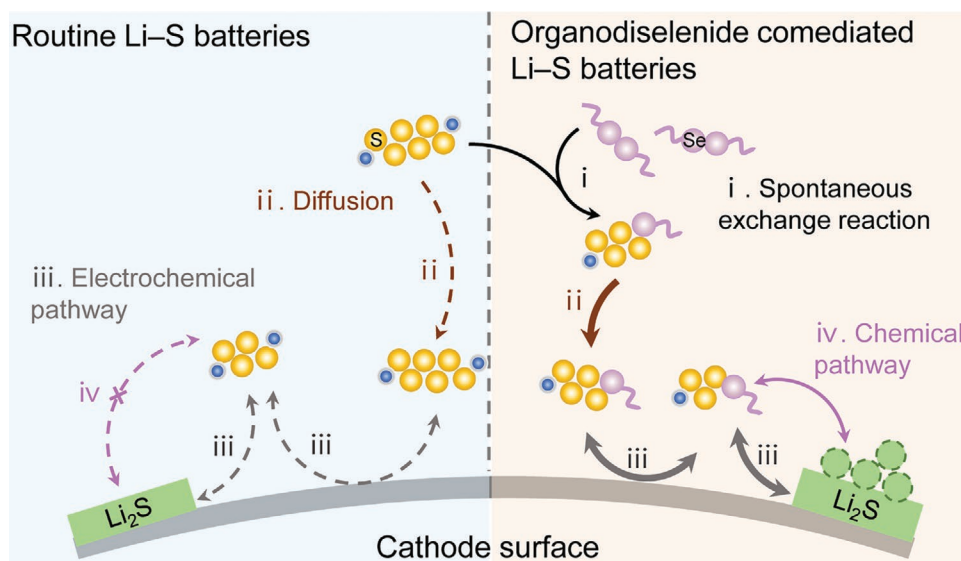


**Figure 1.** Schematic of routine (left) and organodiselenide-comediated (right) reaction pathway for Li-S batteries. Black arrow: spontaneous exchange reaction; brown arrow: diffusion of charged molecules; gray arrows: electrochemical reduction/oxidation; purple arrows: chemical dissociation of polysulfide; thinner dashed arrows: sluggish kinetics; and thicker solid arrows: fast kinetics.

the other hand, benzo[ghi]peryleneimide<sup>[14]</sup> and cobaltocene<sup>[15]</sup> were introduced to mediate the  $\text{Li}_2\text{S}$  deposition process with enhanced discharge capacity. Moreover, fast diffusion and conversion of the extrinsic mediators can also promote the overall sulfur redox kinetics and improve the rate performance. Nevertheless, the extrinsic mediation processes are always accompanied with severe shuttle effect caused by the redox mediators with fast diffusivity.<sup>[16]</sup> Besides, extrinsic redox mediators with only one or two suitable redox couples can only mediate specific conversion processes due to the thermodynamic sequencing, where a full-range mediation of the whole multiphase Li-S reactions can hardly be realized.<sup>[17]</sup> Therefore, it is essential to fundamentally modulate and enhance the intrinsic polysulfide mediators for comprehensively improved battery performances.

Following the above direction, electrolyte optimization is proposed to improve the redox mediation capability of the intrinsic polysulfide mediators via altering their solvation structure.<sup>[18]</sup> Recently, high-donicity solvents, such as dimethyl acetamide,<sup>[19]</sup> dimethyl sulfoxide,<sup>[20]</sup> and propionitrile,<sup>[21]</sup> have been demonstrated to enable improved discharge capacity based on their high solubility toward lithium polysulfides and  $\text{Li}_2\text{S}$ .<sup>[22]</sup> Unfortunately, the violent reactivity of the high-donicity solvents with Li anode hinders stable cycling of the Li-S batteries.<sup>[23]</sup> Alternatively, reducing the solubility of the lithium polysulfides can generally achieve stable cycling, which is mainly conducted through high-concentration or localized high-concentration systems.<sup>[24]</sup> However, such solvation structures essentially scarify the redox mediation capability of polysulfides and impair the sulfur redox kinetics, exhibiting strong dependence on the operating environment such as high temperature and low current density.<sup>[25]</sup>

To essentially promote the redox mediation capability of the intrinsic polysulfide mediators, introducing a redox comediator that modifies the molecular structure of the lithium polysulfides constitutes a feasible strategy. The redox comediator is expected to reversibly react with lithium polysulfides to afford

products with higher redox mediation capability. The products are supposed to facilitate the sulfur redox kinetics as active redox mediators. Following such consideration, selenium in the same VIA group demonstrates reactivity with sulfur and kinetic advantages due to stronger metallicity and electrical conductivity.<sup>[26]</sup> Several organoselenides or carbon-selenium can even function as electrode active materials themselves.<sup>[27]</sup> Therefore, covalent modification of the polysulfides with selenium is expected to increase their redox mediation capability and promote the sulfur redox kinetics, where such methodology remains unexplored and needs to be testified.

Here, based on the principles of the redox comediation strategy, a selenium-based redox comediator is proposed to accelerate the sulfur redox reactions and construct high-performance Li-S batteries (**Figure 1**). Concretely, diphenyl diselenide (DPDSe) dissolved in electrolyte spontaneously reacts with lithium polysulfides and generates soluble lithium phenylseleno polysulfides (LiPhSePSs). The as-produced LiPhSePSs with improved redox mediation capability reduce the dissolution energy barrier and increase the deposition dimension of  $\text{Li}_2\text{S}$  while not damaging lithium metal during cycling. Consequently, the DPDSe comediator endows Li-S batteries with excellent rate performance of  $817 \text{ mA h g}^{-1}$  at 2 C and remarkable cycling stability with ultrathin Li anode. Furthermore, Li-S pouch cells with the DPDSe comediator achieve an actual initial energy density of  $301 \text{ Wh kg}^{-1}$  and 30 stable cycles at 0.05 C.

To reveal the chemical reactions between polysulfides and DPDSe, equimolar amounts of  $\text{Li}_2\text{S}_6$  and DPDSe were mixed to obtain a LiPhSePS solution (denoted as DPDSe +  $\text{Li}_2\text{S}_6$ ), where  $\text{Li}_2\text{S}_6$  was selected as a representative polysulfide redox mediator. The yellow  $\text{Li}_2\text{S}_6$  solution turned red after mixing with pale yellow DPDSe (**Figure 2a**), suggesting the expected chemical reaction occurred. Spectroscopic evidence corresponds well with the visual observation. According to the ultraviolet-visible spectra,  $\text{Li}_2\text{S}_6$  and DPDSe exhibited

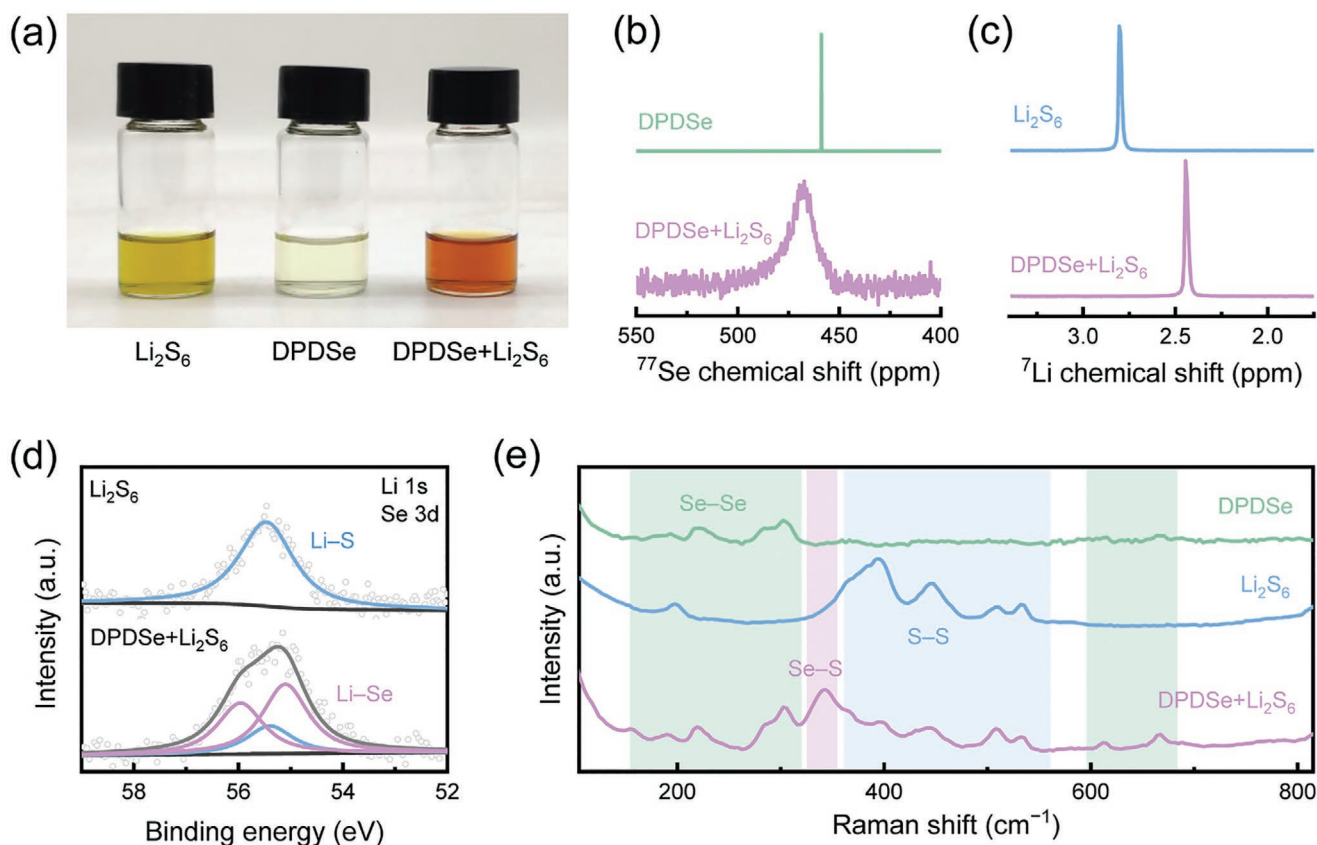


**Figure 2.** Interaction of DPDS with lithium polysulfides. a) Photograph of chemical reaction between  $\text{Li}_2\text{S}_6$  and DPDS solutions. b)  $^{77}\text{Se}$  and c)  $^7\text{Li}$  NMR spectra of the DPDS solution, the  $\text{Li}_2\text{S}_6$  solution, and the mixed DPDS +  $\text{Li}_2\text{S}_6$  solution. d) Li 1s (Se 3d) XPS spectra of  $\text{Li}_2\text{S}_6$  before and after the chemical reaction with DPDS. e) Raman spectra of DPDS and  $\text{Li}_2\text{S}_6$  solutions before and after chemical reaction.

significant absorption peaks at 283 and 311 nm, respectively (Figure S1, Supporting Information). On the contrary, the peak intensity of the mixed sample at 350 nm far exceeded the sum of the pristine DPDS and  $\text{Li}_2\text{S}_6$ , indicating the spontaneous dynamic exchange reaction between the diselenium bond and the disulfide bond. Nuclear magnetic resonance (NMR) spectra of  $^{77}\text{Se}$  also confirm the exchange reaction.<sup>[28]</sup> Before mixing, DPDS showed an apparent resonance at 460 ppm (Figure 2b). After the exchange reaction, the chemical shift of the Se–Se interaction upshifted to 468 ppm which probably resulted from the interaction of Se–S.<sup>[29]</sup> Similarly, in the  $^7\text{Li}$  NMR spectra, the chemical shift signal of  $\text{Li}_2\text{S}_6$  was also shifted from 2.81 to 2.45 ppm (Figure 2c) probably due to the electron transfer from electron-rich Se to Li via the Se–S bonds.

To further demonstrate the chemical reaction between DPDS and lithium polysulfides, the  $\text{Li}_2\text{S}_6$  solutions with or without DPDS were dropped on polypropylene matrix and dried for X-ray photoelectron spectroscopy (XPS) characterization. Pristine  $\text{Li}_2\text{S}_6$  exhibited a typical Li–S bond at 55.5 eV in the Li 1s spectra (Figure 2d).<sup>[30]</sup> In contrast, additional peaks corresponding to the Li–Se bond were deconvoluted for the DPDS +  $\text{Li}_2\text{S}_6$  sample at 55.1 eV (attributing to Se  $3d_{5/2}$ ).<sup>[31]</sup> Moreover, the presence of Se–S bonds was clearly identified by Raman spectroscopy. The pristine  $\text{Li}_2\text{S}_6$  showed typical scattering peaks at 198, 394, 445, 510, and 533  $\text{cm}^{-1}$ , while the

DPDS solution possessed a series of peaks between 155–318 and 587–684  $\text{cm}^{-1}$  (Figure 2e).<sup>[32]</sup> After the exchange reaction, the scattering peak of  $\text{Li}_2\text{S}_6$  at 198  $\text{cm}^{-1}$  disappeared, and the intensity ratios of other peaks also changed significantly. More importantly, a new peak probably belonging to Se–S vibration appeared at 341  $\text{cm}^{-1}$ .<sup>[33]</sup> All the evidences confirm that the reaction between DPDS and  $\text{Li}_2\text{S}_6$  generates seleno polysulfides via spontaneous exchange reactions.

The liquid–solid sulfur reaction kinetics corresponding to  $\text{Li}_2\text{S}$  deposition from dissolved lithium polysulfides were probed to elucidate the comediator effect of DPDS. Following the previous literatures,<sup>[34]</sup> chronoamperometry was conducted to demonstrate the nucleation behaviors of  $\text{Li}_2\text{S}$  on the same conductive substrates with or without DPDS comediators (Figure 3a). The cell comediated by DPDS reached the highest potentiostatic current after 3300 s,  $\approx 9700$  s ahead of the blank cell, proving fast deposition kinetics of  $\text{Li}_2\text{S}$ .<sup>[35]</sup> Meanwhile, due to the modulation of DPDS, the deposition capacity of  $\text{Li}_2\text{S}$  achieved 810  $\text{mAh g}^{-1}$ , which is 2.2 times as much as that of the blank cell. Morphological characteristics of the electrodes revealed the reason for capacity improvement. Unlike film  $\text{Li}_2\text{S}$  deposition directed by the intrinsic polysulfide mediators, the DPDS-comediated  $\text{Li}_2\text{S}$  deposition was thicker and featured a 3D growth characteristic (Figure S2, Supporting Information), which implies higher deposition capacity on limited conductive surfaces.

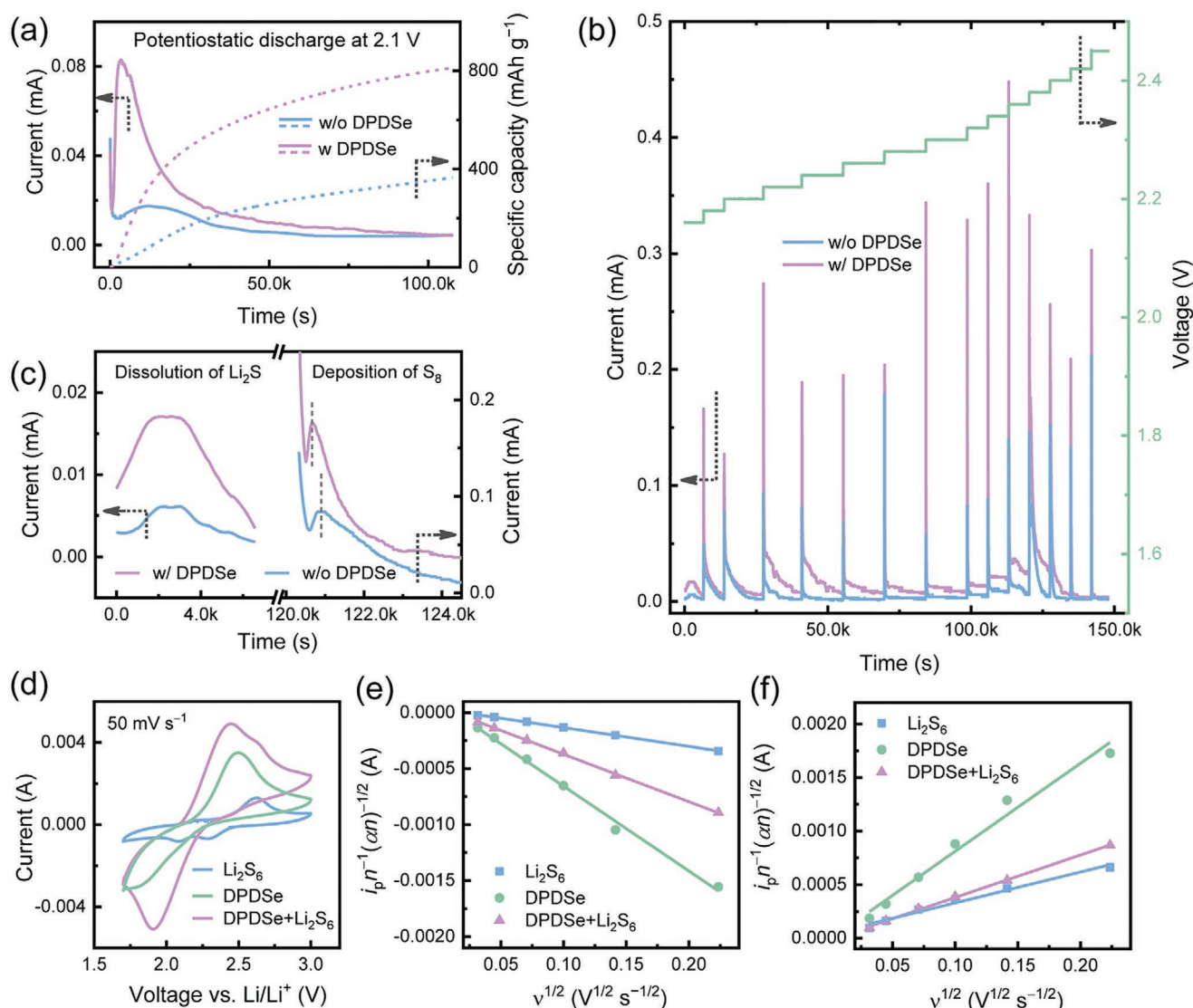


**Figure 3.** Kinetic evaluation of the DPDSer redox mediator toward the sulfur redox reactions. a) Chronoamperometry curves of Li | Li<sub>2</sub>S<sub>8</sub> cells, showing the kinetics of Li<sub>2</sub>S deposition. b) PITT profiles of Li | Li<sub>2</sub>S cells, showing the kinetics of Li<sub>2</sub>S charging to S<sub>8</sub>. c) Partially enlarged view of (b), showing the current responses during Li<sub>2</sub>S dissolution and S<sub>8</sub> deposition. d) CV curves of the Li | DPDSer, Li | Li<sub>2</sub>S<sub>6</sub>, and Li | DPDSer + Li<sub>2</sub>S<sub>6</sub> cells at the scan rate of 50 mV s<sup>-1</sup>. e, f) The diffusion coefficients of DPDSer, Li<sub>2</sub>S<sub>6</sub>, and their products corresponding to the reduction (e) and the oxidation (f) processes.

Generally, the delithiation of insulated Li<sub>2</sub>S is severely hindered due to the passivated conductive interface and the depletion of intrinsic polysulfide mediators at the beginning of charge.<sup>[36]</sup> To probe the mediation effect of DPDSer on the Li<sub>2</sub>S oxidation process, potentiostatic intermittent titration technique (PITT) was conducted (Figure 3b).<sup>[37]</sup> The Li<sub>2</sub>S charging PITT process can be generally divided into three parts regarding solid–liquid, liquid–liquid, and liquid–solid conversions. The first charge stage at 2.16 V corresponds to the oxidation of Li<sub>2</sub>S to soluble short-chain lithium polysulfides. The integrated area of the current peak represents the Li<sub>2</sub>S dissolution capacity (Figure 3c). The DPDSer-mediated cell delivered a Li<sub>2</sub>S dissolution capacity of 35 mAh g<sup>-1</sup>, which greatly exceeded the blank cell (Figure S3, Supporting Information). Similarly, in the second conversion stage from 2.18 to 2.36 V corresponding to oxidation from short-chain to long-chain lithium polysulfides,

the DPDSer-mediated cell also provided significantly higher current responses. The total charging capacity within this range is 1009 mAh g<sup>-1</sup>, equivalent to 2.3 times as that of the blank cell. Following that, solid S<sub>8</sub> began to precipitate at 2.40 V manifested by the peak-shape current response that suggests phase transition processes. The DPDSer-cell reached its current peak after ≈300 s and achieved a deposition capacity of 178 mAh g<sup>-1</sup>. In contrast, the peak time of the blank cell was delayed to ≈600 s with an integrated area reduced to 52% (Figure S3, Supporting Information), implying the sluggish sulfur redox kinetics and deficiency of the intrinsic polysulfide mediators. The charging PITT characterization demonstrates the critical role of the DPDSer mediator in promoting the inert lithium polysulfide mediators for faster sulfur redox kinetics.

Symmetric cells with Li<sub>2</sub>S<sub>6</sub> electrolyte and carbon paper current collectors were assembled to investigate the regulation

effect of DPDSe on the liquid–liquid conversion kinetics. The electrochemical impedance spectroscopy of the symmetrical cells showed that DPDSe reduces the charge transfer impedance from 165 to 26  $\Omega$  (Figure S4a, Supporting Information), demonstrating faster conversion kinetics rendered by the LiPhSePS redox mediators. Due to direct effect of impedance reduction on the polysulfide conversion kinetics at the conductive interface, the DPDSe + Li<sub>2</sub>S<sub>6</sub> cell exhibited significantly increased redox current responses at the polarization of 0.8 V increasing from 1 to 29 mA (Figure S4b, Supporting Information).

In addition to the charge transfer kinetics at reactive interfaces, diffusion kinetics of the active materials also greatly affects the overall electrochemical performances. Li | Li<sub>2</sub>S<sub>6</sub>, Li | DPDSe and Li | DPDSe+Li<sub>2</sub>S<sub>6</sub> cells were assembled to measure the diffusivity of the active materials using cyclic voltammogram (CV) at different scan rates (Figure S5, Supporting Information). The peak potential difference gradually increased with raising scan rates due to the mass-transfer limitation. Under the scan rate of 50 mV s<sup>-1</sup>, the original two pairs of the redox characteristic peaks of the Li<sub>2</sub>S<sub>6</sub> cell were overlapped into one pair in the DPDSe + Li<sub>2</sub>S<sub>6</sub> cell due to the reaction of Li<sub>2</sub>S<sub>6</sub> and DPDSe (Figure 3d). More importantly, the DPDSe + Li<sub>2</sub>S<sub>6</sub> cell provided higher redox currents compared with the Li<sub>2</sub>S<sub>6</sub> or the DPDSe cells and even greater than the sum of the two (23% and 197% higher

for the oxidation and the reduction peak, respectively), indicating higher electrochemical reactivity provided by the products of the Se–S exchange reactions. Using the well-known Randles–Sevcik equation, the peaks corresponding to the oxidation and reduction processes were selected to fit the diffusion coefficients.<sup>[38]</sup> The DPDSe cell showed a diffusion coefficient of  $4.5 \times 10^{-8}$  and  $5.3 \times 10^{-8}$  cm<sup>2</sup> s<sup>-1</sup> that is about 20.5 and 8.2 times higher in reduction and oxidation process compared with the pristine Li<sub>2</sub>S<sub>6</sub> cell, respectively (Figures 3e and 3f). Accordingly, the diffusion kinetics of the DPDSe + Li<sub>2</sub>S<sub>6</sub> cell was also enhanced remarkably with a diffusion coefficient of  $1.4 \times 10^{-8}$  and  $1.2 \times 10^{-8}$  cm<sup>2</sup> s<sup>-1</sup> for the two electrochemical processes, about 6.4 and 1.8 times than the pristine Li<sub>2</sub>S<sub>6</sub> cells, respectively (Figure S6, Supporting Information). Even in actual Li–S cells, DPDSe still promoted the diffusion process of polysulfides (Figures S7 and S8, Supporting Information).<sup>[39]</sup> The promotion of the mass-transfer process also illustrates possible reasons for the enhancement of the heterogeneous and homogeneous electrochemical reactions of the sulfur-containing species probed above.

To further understand the origin of the kinetic advances of the LiPhSePSs over lithium polysulfides, first-principles calculations were conducted toward several representative molecules regarding Li<sub>2</sub>S<sub>4–8</sub> and LiPhSePS<sub>4–8</sub>. The optimized molecular configurations are shown in Figure 4a. A strong intramolecular

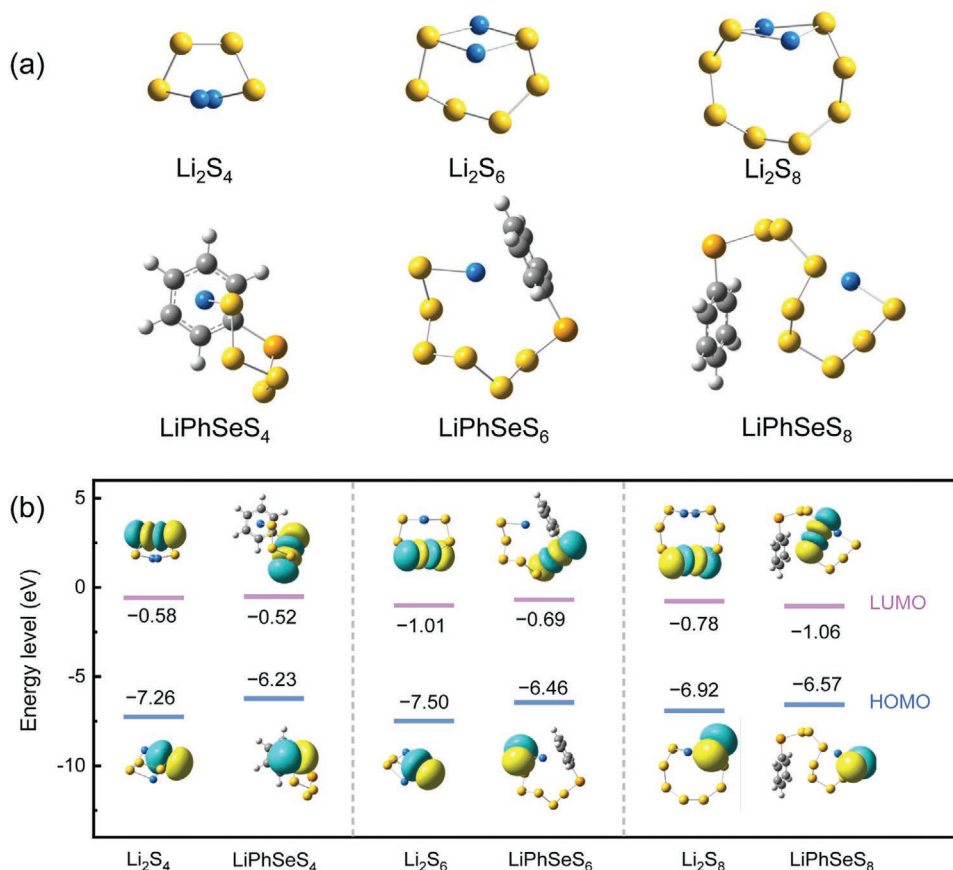


**Figure 4.** Simulation results of LiPSs and LiPhSePSs. a) Optimized molecular structures and b) LUMO and HOMO energy levels of different Li<sub>2</sub>S<sub>n</sub> and LiPhSeS<sub>n</sub>,  $n = 8, 6$ , or  $4$ . The hydrogen, lithium, carbon, sulfur, and selenium atoms are marked with white, blue, gray, yellow, and orange, respectively. The cyan and yellow regions represent the positive and negative parts of the LUMO and HOMO isosurface, respectively (isovalue: 0.02). The results of Li<sub>2</sub>S<sub>n</sub> are from our previous reports.<sup>[40]</sup>

interaction between lithium and benzene ring was identified in  $\text{LiPhSeS}_6$  and  $\text{LiPhSeS}_4$ , while C–S interactions were dominant in  $\text{LiPhSeS}_8$  due to the long sulfur chain. To further reveal the redox properties of the molecules, the energy levels of the lowest unoccupied molecular orbital (LUMO) and the highest occupied molecular orbital (HOMO) were analyzed. The  $\text{LiPhSeS}_n$ s afford different HOMO and LUMO energies in comparison with the corresponding lithium polysulfides with the same sulfur atoms, suggesting varied redox properties and mediation capability during discharge and charge (Figure 4b). Moreover, the LUMOs of  $\text{LiPhSeS}_6$  and  $\text{LiPhSeS}_4$  changed from middle S–S bond in  $\text{Li}_2\text{S}_6$  and  $\text{Li}_2\text{S}_4$  to Se–S bond due to the Li–Ph interactions. Notably, the above simulations only provide thermodynamic results while the  $\text{LiPhSePS}$ s and lithium polysulfides in working Li–S batteries are under kinetic control with different concentration and spatial distribution varied with depth of charge and discharge. Nevertheless, the above simulation results afford the possibility to fundamentally understand the chemistry of DPDS<sub>e</sub>-comediated processes toward the sulfur redox reactions.

The rapid polysulfide redox reactions comediated by DPDS<sub>e</sub> render superb rate performance in working Li–S batteries. The DPDS<sub>e</sub>-comediated Li–S cells achieved capacities of 1218, 1091, 961, 889, and 817 mAh g<sup>-1</sup> at 0.1, 0.2, 0.5, 1, and 2 C (1 C = 1672 mA g<sub>S</sub><sup>-1</sup>), respectively, 13–214% higher than the control cells (Figure S9, Supporting Information, and Figure 5a). The galvanostatic discharge–charge curves at different rates revealed the origin of the high-rate capability (Figure S10, Supporting Information). The DPDS<sub>e</sub> comediator significantly extended the second discharge plateaus at 0.1 C and lowers the polarization at higher rates to afford two-plateau discharge curves, consistent with previous demonstrations in kinetics experiments. Furthermore, the insulating  $\text{Li}_2\text{S}$  exhibited a high potential barrier at the initial delithiation process due to the depletion of intrinsic polysulfide mediators in the control cell (Figure 5b), while the comediators of DPDS<sub>e</sub> eliminated the potential barrier and exhibited a smooth charging curve. The above advantages all contribute to improved rate performances of Li–S batteries.

The DPDS<sub>e</sub> comediators strategy also favors long-term cycling stability at 0.5 C with 33 μm ultrathin lithium metal anode corresponding to a negative/positive electrode capacity ratio (N/P ratio) of 4.5 (Figure 5c). Initially, the DPDS<sub>e</sub> comediators cell delivered a capacity of 1056 mAh g<sup>-1</sup>. After extensive 350 cycles, a capacity of 720 mAh g<sup>-1</sup> was preserved, corresponding to a cyclic decay rate of 0.091% per cycle. More remarkably, the Coulombic efficiency was maintained above 93%, indicating that the faster-diffusing  $\text{LiPhSePS}$ s did not exacerbate the shuttle effect. However, the blank cell only provided an initial capacity of 979 mAh g<sup>-1</sup> and a cyclic decay rate of 0.156% per cycle, which exhibited a sharp capacity decay after 150 cycles probably due to the deposition of a “dead sulfur” layer and sharply deteriorated voltage polarization (Figures S11 and S12, Supporting Information).<sup>[41]</sup> Furthermore, Li anodes with DPDS<sub>e</sub> after 50 cycles exhibited a more flatter morphology with a thinner deposition layer than the anode without DPDS<sub>e</sub> (Figure S13, Supporting Information). The high capacity of the DPDS<sub>e</sub>-cells can be attributed to the effective and sustainable comediators process, and the high stability approximately

benefits from the protective effect of the aromatic group on the lithium anode.<sup>[42]</sup> Nevertheless, excessive concentration of DPDS<sub>e</sub> led to sharp capacity decay due to deteriorated shuttle effect and lithium anode corrosion (Figure S14, Supporting Information). An optimal concentration of the DPDS<sub>e</sub> comediator is therefore highly important to cooperatively promote Li–S battery performances.

Previous CV results indicate that DPDS<sub>e</sub> possesses electrochemical activity within the electrochemical window of Li–S batteries. To exclude the contribution of DPDS<sub>e</sub> to the total capacity, a Li | DPDS<sub>e</sub> cell was assembled with 100 mmol L<sup>-1</sup> DPDS<sub>e</sub> in catholyte. Within 350 cycles, DPDS<sub>e</sub> only delivered a capacity of about 5 mAh g<sup>-1</sup> at a current density of 0.2 mA cm<sup>-2</sup> calculated with a sulfur loading of 1.2 mg<sub>S</sub> cm<sup>-2</sup> (Figure S15, Supporting Information). Therefore, the discharge capacity contributed by DPDS<sub>e</sub> is negligible relative to the capacity provided by sulfur.

To build a high-energy-density Li–S battery, increasing the sulfur areal loading is essential whereas the amount of DPDS<sub>e</sub> remains unchanged to explore the comediators effect. Even if the sulfur loading was raised to 5.0 mg<sub>S</sub> cm<sup>-2</sup>, cells with DPDS<sub>e</sub> still delivered an initial capacity of 924 mAh g<sup>-1</sup> at 0.1 C (Figure 5d). After 55 cycles, a capacity of 765 mAh g<sup>-1</sup> can still be provided. In contrast, the routine cell only delivered a discharge capacity of about 700 mAh g<sup>-1</sup> over 55 cycles. Similar to the low-sulfur-loading conditions, the high-sulfur-loading Li–S cells comediators by DPDS<sub>e</sub> exhibited extended charge/discharge plateaus and reduced initial charge potential barrier (Figure S16a, Supporting Information). During discharge, the ratio of low- and high-plateau capacities ( $Q_{\text{low}}/Q_{\text{high}}$ ) is usually used to evaluate the conversion efficiency of polysulfides to  $\text{Li}_2\text{S}$ . The Li–S cells with DPDS<sub>e</sub> provided a  $Q_{\text{low}}/Q_{\text{high}}$  of 2.47, 10% higher than that without DPDS<sub>e</sub> (Figure S16b, Supporting Information), indicating the remarkable promotion for  $\text{Li}_2\text{S}$  deposition.

To further verify the feasibility of DPDS<sub>e</sub> to promote electrochemical performances in practical high-energy-density batteries, Li–S pouch cells with a design capacity of 1.5 Ah were assembled (Figure 5e). The DPDS<sub>e</sub>-comediators pouch cell provided an initial specific capacity of 1322 mAh g<sup>-1</sup> and an initial energy density of 301 Wh kg<sup>-1</sup> at 0.05 C. Moreover, the pouch cell with DPDS<sub>e</sub> still maintained an energy density of 265 Wh kg<sup>-1</sup> after 30 cycles. In the galvanostatic charge–discharge profiles of the pouch cell, DPDS<sub>e</sub> significantly improves the conversion efficiency of polysulfides to  $\text{Li}_2\text{S}$  with a  $Q_{\text{low}}/Q_{\text{high}}$  above 2.6, which is similar to the phenomenon observed in coin cells (Figure S17, Supporting Information). The above enhancement can be attributed to the advantages of the  $\text{LiPhSePS}$ s compared with the intrinsic polysulfide mediators regarding: 1) the  $\text{LiPhSePS}$ s break the polysulfide diffusion limit and enable thorough  $\text{Li}_2\text{S}$  deposition/dissolution; 2) the  $\text{LiPhSePS}$ s enhance the conversion kinetics of lithium polysulfides and accelerate the sulfur redox reactions; and 3) the intervention of the  $\text{LiPhSePS}$ s modulates the original chemical/electrochemical balance and realizes high-capacity and high-reversible deposition of  $\text{Li}_2\text{S}$ .

In summary, a DPDS<sub>e</sub> comediators strategy is proposed to facilitate the sulfur redox reaction kinetics for high-rate and high-capacity Li–S batteries. Severing as a redox comediator, DPDS<sub>e</sub> chemically reacts with lithium polysulfides and

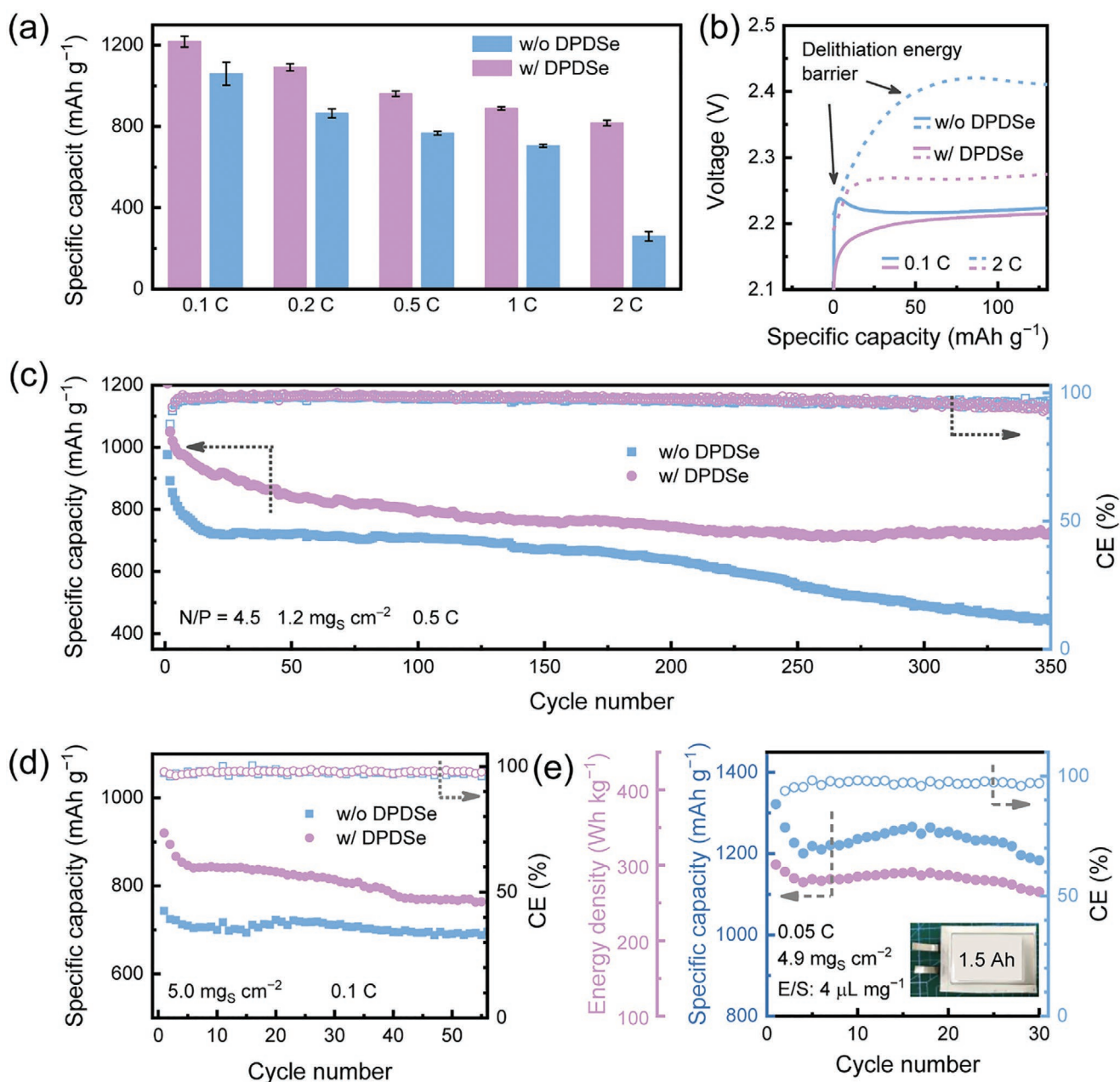


**Figure 5.** Electrochemical performance of Li-S batteries mediated by DPDSe. a) Rate performance showing capacities in average. b) Initial galvanostatic charge profiles at various current densities. c) Long-term cycling with a N/P ratio of 4.5 at 0.5 C. The sulfur loading in (a)–(c) was  $1.2 \text{ mg}_S \text{ cm}^{-2}$ . d) Cycling performance of Li-S cells with high sulfur loading of  $5.0 \text{ mg}_S \text{ cm}^{-2}$ . e) Cycling performance of Li-S pouch cells with high sulfur loading of  $4.9 \text{ mg}_S \text{ cm}^{-2}$  and E/S ratio of  $4.0 \mu\text{L mg}_S^{-1}$  at 0.05 C.

generates LiPhSePSs with higher mediation capabilities. The DPDSe comediator reduces the energy barriers for multiphase sulfur conversions, alters  $\text{Li}_2\text{S}$  deposition to permit higher deposition capacity, and promises faster diffusion kinetics. The Li-S batteries mediated by DPDSe exhibited superb rate performance with a capacity of  $817 \text{ mAh g}^{-1}$  at 2 C and remarkable cycling stability with ultrathin Li anodes. Moreover, Li-S pouch cells with the DPDSe comediator achieve an actual initial energy density of  $301 \text{ Wh kg}^{-1}$  and 30 stable cycles. This work not only proposes a novel redox

commediation strategy and an effective DPDSe comediator to promote Li-S battery performances under practical conditions, but also inspires further exploration in mediating multielectron and multiphase energy processes for practical high-energy-density systems.

### Supporting Information

Supporting Information is available from the Wiley Online Library or from the author.

## Acknowledgements

This work was supported by the Beijing Natural Science Foundation (JQ20004), National Natural Science Foundation of China (21776019 and U1801257), National Key Research and Development Program (2016YFA0202500), and Scientific and Technological Key Project of Shanxi Province (20191102003). The authors acknowledged the support from Tsinghua National Laboratory for Information Science and Technology for theoretical simulations. The authors thank Jin Xie, Chang-Xin Zhao, Ye Xiao, Xue-Qiang Zhang, and Prof. Hong Yuan for helpful discussion.

## Conflict of Interest

The authors declare no conflict of interest.

## Keywords

lithium polysulfides, lithium–sulfur batteries, organodiselenides, redox mediators, sulfur redox kinetics

Received: October 25, 2020

Revised: December 6, 2020

Published online: February 15, 2021

- [1] a) B. Dunn, H. Kamath, J. M. Tarascon, *Science* **2011**, *334*, 928; b) J. W. Choi, D. Aurbach, *Nat. Rev. Mater.* **2016**, *1*, 16013.
- [2] A. Bhargav, J. R. He, A. Gupta, A. Manthiram, *Joule* **2020**, *4*, 285.
- [3] H. L. Pan, J. Z. Chen, R. G. Cao, V. Murugesan, N. N. Rajput, K. S. Han, K. Persson, L. Estevez, M. H. Engelhard, J. G. Zhang, K. T. Mueller, Y. Cui, Y. Y. Shao, J. Liu, *Nat. Energy* **2017**, *2*, 813.
- [4] a) T. Y. Lei, W. Chen, W. Q. Lv, J. W. Huang, J. Zhu, J. W. Chu, C. Y. Yan, C. Y. Wu, Y. C. Yan, W. D. He, J. Xiong, Y. R. Li, C. L. Yan, J. B. Goodenough, X. F. Duan, *Joule* **2018**, *2*, 2091; b) M. Li, Z. Chen, T. P. Wu, J. Lu, *Adv. Mater.* **2018**, *30*, 1801190.
- [5] a) Z. Zhang, D. Luo, G. R. Li, R. Gao, M. Li, S. Li, L. Zhao, H. Z. Dou, G. B. Wen, S. Sy, Y. F. Hu, J. D. Li, A. P. Yu, Z. W. Chen, *Matter* **2020**, *3*, 920; b) C. B. Sun, Y. Q. Liu, J. Z. Sheng, Q. K. Huang, W. Lv, G. M. Zhou, H. M. Cheng, *Mater. Horiz.* **2020**, *7*, 2487; c) H. Tang, L. You, J. W. Liu, S. Wang, P. Wang, C. Feng, Z. P. Guo, *ACS Appl. Mater. Interfaces* **2019**, *11*, 18448; d) X. D. Hong, R. Wang, Y. Liu, J. W. Fu, J. Liang, S. X. Dou, *J. Energy Chem.* **2020**, *42*, 144; e) J. E. Knoop, S. Ahn, *J. Energy Chem.* **2020**, *47*, 86.
- [6] Y. C. Lu, Q. He, H. A. Gasteiger, *J. Phys. Chem. C* **2014**, *118*, 5733.
- [7] Q. Zou, Y. C. Lu, *J. Phys. Chem. Lett.* **2016**, *7*, 1518.
- [8] M. Cuisinier, P. E. Cabelguen, S. Evers, G. He, M. Kolbeck, A. Garsuch, T. Bolin, M. Balasubramanian, L. F. Nazar, *J. Phys. Chem. Lett.* **2013**, *4*, 3227.
- [9] H. J. Peng, J. Q. Huang, X. Y. Liu, X. B. Cheng, W. T. Xu, C. Z. Zhao, F. Wei, Q. Zhang, *J. Am. Chem. Soc.* **2017**, *139*, 8458.
- [10] a) L. Kong, Q. Jin, J. Q. Huang, L. D. Zhao, P. Li, B. Q. Li, H. J. Peng, X. T. Zhang, Q. Zhang, *Energy Technol.* **2019**, *7*, 1900111; b) C. Weller, S. Thieme, P. Hartel, H. Althues, S. Kaskel, *J. Electrochem. Soc.* **2017**, *164*, A3766.
- [11] a) Q. Pang, X. Liang, C. Y. Kwok, L. F. Nazar, *Nat. Energy* **2016**, *1*, 16132; b) H. Ye, J. Y. Lee, *Small Methods* **2020**, *4*, 1900864.
- [12] S. Meini, R. Elazari, A. Rosenman, A. Garsuch, D. Aurbach, *J. Phys. Chem. Lett.* **2014**, *5*, 915.
- [13] Y. Tsao, M. Lee, E. C. Miller, G. P. Gao, J. Park, S. C. Chen, T. Katsumata, H. Tran, L. W. Wang, M. F. Toney, Y. Cui, Z. N. Bao, *Joule* **2019**, *3*, 872.
- [14] L. C. Gerber, P. D. Frischmann, F. Y. Fan, S. E. Doris, X. Qu, A. M. Scheuermann, K. Persson, Y. M. Chiang, B. A. Helms, *Nano Lett.* **2016**, *16*, 549.
- [15] M. Zhao, H. J. Peng, J. Y. Wei, J. Q. Huang, B. Q. Li, H. Yuan, Q. Zhang, *Small Methods* **2019**, *4*, 1900344.
- [16] Z. W. Zhang, H. J. Peng, M. Zhao, J. Q. Huang, *Adv. Funct. Mater.* **2018**, *28*, 1707536.
- [17] P. D. Frischmann, L. C. H. Gerber, S. E. Doris, E. Y. Tsai, F. Y. Fan, X. H. Qu, A. Jain, K. A. Persson, Y. M. Chiang, B. A. Helms, *Chem. Mater.* **2015**, *27*, 6765.
- [18] a) T. Yang, T. Qian, J. Liu, N. Xu, Y. Li, N. Grundish, C. Yan, J. B. Goodenough, *ACS Nano* **2019**, *13*, 9067; b) M. Cuisinier, P. E. Cabelguen, B. D. Adams, A. Garsuch, M. Balasubramanian, L. F. Nazar, *Energy Environ. Sci.* **2014**, *7*, 2697; c) S. Y. Lang, R. J. Xiao, L. Gu, Y. G. Guo, R. Wen, L. J. Wan, *J. Am. Chem. Soc.* **2018**, *140*, 8147.
- [19] M. Cuisinier, C. Hart, M. Balasubramanian, A. Garsuch, L. F. Nazar, *Adv. Energy Mater.* **2015**, *5*, 1401801.
- [20] a) H. L. Pan, X. L. Wei, W. A. Henderson, Y. Y. Shao, J. Z. Chen, P. Bhattacharya, J. Xiao, J. Liu, *Adv. Energy Mater.* **2015**, *5*, 1500113; b) X. Yu, A. Manthiram, *Phys. Chem. Chem. Phys.* **2015**, *17*, 2127.
- [21] Z. J. Li, Y. C. Zhou, Y. Wang, Y. C. Lu, *Adv. Energy Mater.* **2018**, *9*, 1802207.
- [22] G. Zhang, H. J. Peng, C. Z. Zhao, X. Chen, L. D. Zhao, P. Li, J. Q. Huang, Q. Zhang, *Angew. Chem., Int. Ed.* **2018**, *57*, 16732.
- [23] H. Shin, M. Baek, A. Gupta, K. Char, A. Manthiram, J. W. Choi, *Adv. Energy Mater.* **2020**, *10*, 2001456.
- [24] a) C. Weller, J. Pampel, S. Dörfler, H. Althues, S. Kaskel, *Energy Technol.* **2019**, *7*, 1900625; b) Q. Pang, A. Shyamsunder, B. Narayanan, C. Y. Kwok, L. A. Curtiss, L. F. Nazar, *Nat. Energy* **2018**, *3*, 783.
- [25] a) C. W. Lee, Q. Pang, S. Ha, L. Cheng, S. D. Han, K. R. Zavadil, K. G. Gallagher, L. F. Nazar, M. Balasubramanian, *ACS Cent. Sci.* **2017**, *3*, 605; b) L. Cheng, L. A. Curtiss, K. R. Zavadil, A. A. Gewirth, Y. Shao, K. G. Gallagher, *ACS Energy Lett.* **2016**, *1*, 503.
- [26] a) K. Wang, Y. P. Guan, Z. Q. Jin, W. K. Wang, A. B. Wang, *J. Energy Chem.* **2019**, *39*, 249; b) J. Q. Zhou, T. Qian, N. Xu, M. F. Wang, X. Y. Ni, X. J. Liu, X. W. Shen, C. L. Yan, *Adv. Mater.* **2017**, *29*, 1701294; c) G. L. Xu, H. Sun, C. Luo, L. Estevez, M. H. Zhuang, H. Gao, R. Amine, H. Wang, X. Y. Zhang, C. J. Sun, Y. Z. Liu, Y. Ren, S. M. Heald, C. S. Wang, Z. H. Chen, K. Amine, *Adv. Energy Mater.* **2018**, *9*, 1802235; d) P. P. Dong, K. S. Han, J. I. Lee, X. H. Zhang, Y. Cha, M. K. Song, *ACS Appl. Mater. Interfaces* **2018**, *10*, 29565; e) S. Susarla, A. B. Puthirath, T. Tsafack, D. Salpekar, G. Babu, P. M. Ajayan, *ACS Appl. Mater. Interfaces* **2020**, *12*, 1005.
- [27] a) J. T. Lee, H. Kim, M. Oschatz, D. C. Lee, F. Wu, H. T. Lin, B. Zdyrko, W. I. Cho, S. Kaskel, G. Yushin, *Adv. Energy Mater.* **2015**, *5*, 1400981; b) Y. Cui, J. D. Ackerson, Y. Ma, A. Bhargav, J. A. Karty, W. Guo, L. Zhu, Y. Z. Fu, *Adv. Funct. Mater.* **2018**, *28*, 1801791; c) Y. Jin, K. Liu, J. Lang, X. Jiang, Z. Zheng, Q. Su, Z. Huang, Y. Long, C. A. Wang, H. Wu, Y. Cui, *Joule* **2020**, *4*, 262; d) W. Guo, A. Bhargav, J. Ackerson, Y. Cui, Y. Ma, Y. Z. Fu, *Chem. Commun.* **2018**, *54*, 8873.
- [28] F. Q. Fan, S. B. Ji, C. X. Sun, C. Liu, Y. Yu, Y. Fu, H. P. Xu, *Angew. Chem., Int. Ed.* **2018**, *57*, 16426.
- [29] R. S. Laitinen, P. Pekonen, Y. Hiltunen, T. A. Pakkanen, *Acta Chem. Scand.* **1989**, *43*, 436.
- [30] H. J. Peng, Z. W. Zhang, J. Q. Huang, G. Zhang, J. Xie, W. T. Xu, J. L. Shi, X. Chen, X. B. Cheng, Q. Zhang, *Adv. Mater.* **2016**, *28*, 9551.
- [31] H. Yuan, H. J. Peng, B. Q. Li, J. Xie, L. Kong, M. Zhao, X. Chen, J. Q. Huang, Q. Zhang, *Adv. Energy Mater.* **2019**, *9*, 1802768.
- [32] J. D. McBrayer, T. E. Beechem, B. R. Perdue, C. A. Apblett, F. H. Garzon, *J. Electrochem. Soc.* **2018**, *165*, A876.
- [33] B. Yuan, W. Zhu, I. Hung, Z. Gan, B. Aitken, S. Sen, *J. Phys. Chem. B* **2018**, *122*, 12219.
- [34] F. Y. Fan, W. C. Carter, Y. M. Chiang, *Adv. Mater.* **2015**, *27*, 5203.

- [35] B. Q. Li, H. J. Peng, X. Chen, S. Y. Zhang, J. Xie, C. X. Zhao, Q. Zhang, *CCS Chem.* **2019**, *1*, 128.
- [36] G. M. Zhou, H. Z. Tian, Y. Jin, X. Y. Tao, B. F. Liu, R. F. Zhang, Z. W. Seh, D. Zhuo, Y. Y. Liu, J. Sun, J. Zhao, C. X. Zu, D. S. Wu, Q. F. Zhang, Y. Cui, *Proc. Natl. Acad. Sci. USA* **2017**, *114*, 840.
- [37] B. Q. Li, L. Kong, C. X. Zhao, Q. Jin, X. Chen, H. J. Peng, J. L. Qin, J. X. Chen, H. Yuan, Q. Zhang, J. Q. Huang, *InfoMat* **2019**, *1*, 533.
- [38] J. Hea, G. Hartmann, M. Lee, G. S. Hwang, Y. F. Chen, A. Manthiram, *Energy Environ. Sci.* **2019**, *12*, 344.
- [39] a) Z. Q. Ye, Y. Jiang, L. Li, F. Wu, R. J. Chen, *Adv. Mater.* **2020**, *32*, 2002168; b) H. Zhang, M. Zou, W. Zhao, Y. Wang, Y. Chen, Y. Wu, L. Dai, A. Cao, *ACS Nano* **2019**, *13*, 3982.
- [40] M. Zhao, B. Q. Li, X. Chen, J. Xie, H. Yuan, J. Q. Huang, *Chem* **2020**, *6*, 3297.
- [41] C. Qi, Z. Li, C. Sun, C. Chen, J. Jin, Z. Wen, *ACS Appl. Mater. Interfaces* **2020**, *12*, 49626.
- [42] a) X. X. Yan, H. Zhang, M. L. Huang, M. Z. Qu, Z. K. Wei, *ChemSusChem* **2019**, *12*, 2263; b) G. Li, Q. Huang, X. He, Y. Gao, D. Wang, S. H. Kim, D. Wang, *ACS Nano* **2018**, *12*, 1500.